Transparent-conductive-oxide (TCO) buffer layer effect on resistive switching process in metal/TiO_2/TCO/metal assemblies

E O Filatova[1], **A P Baraban**[1], **A S Konashuk**[1], **M A Konyushenko**[1], **A A Selivanov**[1], **A A Sokolov**[1,2], **F Schaefers**[2] and **V E Drozd**[1]

[1] Institute of Physics, St. Petersburg State University, Ul'yanovskaya Str. 1, Peterhof, 198504, St. Petersburg, Russia
[2] Helmholtz-Zentrum Berlin für Materialien und Energie GmbH, Albert Einstein Str. 15, 12489, Berlin, Germany

Email: feo@ef14131.spb.edu

The effect of transparent-conductive-oxide (TCO) buffer layer on the insulator matrix and on the resistive switching process in the metal/TiO_2/TCO/metal assembly was studied depending on the material of TCO (ITO - $(In_2O_3)_{0.9}(SnO_2)_{0.1}$ or SnO_2 or ZnO). First time electro-physical studies and near edge x-ray absorption fine structure (NEXAFS) studies were carried out jointly and in the same point of the sample providing the direct experimental evidence that switching process influences strongly the lowest unoccupied bands and local atomic structure of the TiO_2 layers. It was established that TCO layer in metal/TiO_2/TCO/metal assembly is an additional source of oxygen vacancies for TiO_2 film. The R_L (R_H) states are achieved presumably with formation (rupture) of electrically conductive path of oxygen vacancies. The inserting the Al_2O_3 thin layer between TiO_2 and TCO layers restricts to some extent processes of migration of oxygen ions and vacancies and does not permit to realize the anti-clockwise bipolar resistive switching in Au/TiO_2/Al_2O_3/ITO/Au assembly. The greatest value of the ratio R_H/R_L is observed for assembly with SnO_2 buffer layer that will provide to implement the maximum set of intermediate states (recording analog data) and increases the density of information recording in this case.

Keywords: Resistive switching, transparent-conductive-oxide, buffer layer, NEXAFS, I-V characteristics, oxygen vacancies

1. Introduction

Relentless downscaling of microelectronic devices had already brought the size of their critical parts to the range of few nanometers and continues to challenge scientists and technologists. Developing nanoscale memory-bit cells [1,2] for non-volatile random access memory (NVRAM) is one key technological step now. Among the many candidates for the next-generation non-volatile memory based on a non-charge mechanism, resistance-switching random access memory (RRAM) has attracted attention as an essential step towards new era of non-Boolean neuromorphic computing [3,4]. The main idea of RRAM connects with creation of passive circuit element memristor (short name of memory resistor) [5-7]. As follows from [5] the memristor with memristance M provides a functional dependence between flux φ and charge q $d\varphi = M dq$. In special case when M is itself a function of the charge, other words, the resistance of the material depends on the charge passing through it a new circuit functions such as resistive switching are opened.

The mechanism of resistance switching and charge transport is still under debate. In the review [8] three different types of the resistive switching (an electrochemical metallization mechanism, a valence change mechanism, a thermochemical mechanism) are described. The valence change mechanism occurs in binary oxides and perovskite oxides and is triggered by migration of oxygen anions. The change of the stoichiometry is expressed by a valence change of the cation sublattice and as a consequence leads to change in the electronic conductivity. In the thermochemical mechanism a change of stoichiometry occurs due to a current-induced increase of the temperature. The electrochemical metallization mechanism relies on an electrochemically active electrode metal.

Many binary transition metal oxides [7-15] as well as multinary oxides with at least one transition metal sublattice [8, 16-18] show resistive switching. The oxide-based elements demonstrate high speed switching, the possibility of obtaining intermediate resistance values and sufficiently stable multilevel switch. The observed resistive switching in such elements occurs due to the presence in these materials of the various defects and impurities which alter the electron transport in the material. The titanium oxide is considered as the most promising switching material [19-21] due to existence of a continuous homologous series of oxides of TiO to TiO_2, the existence of thermal-chemical switching mode [22] and minimum value of switching time (5 ns) [23]. Note that to provide a switching control of such elements it is necessary to create defects in materials, either during or after fabrication of the element through electric field effect on the pristine structure (electroforming process) [8].

It has been established in [24-26] that inserting a thin buffer layer between the substrate and dielectric film allows to affect the self-organization and the properties of the active layer. Taking into account a high concentration of oxygen vacancies in transparent-conductive-oxide (TCO) films one can assume that TCO layers in metal/TiO_2/TCO/metal assembly will be an additional source of oxygen vacancies for TiO_2 film. Earlier we have revealed that such assemblies demonstrate the memristors effect after synthesis (without additional annealing) that allows moving closer to understanding the nature of memristor effect. Also it was established that after switching process these structures can be retained for a long time.

In view of the foregoing, the goal of the current paper is a study of the effect of TCO buffer layers on the insulator matrix in the metal/TiO_2/TCO/metal assembly and on the resistive switching process. In order to gain inside into the electronic structure of the TiO_2 film for the first time the electro-physical studies and the x-ray spectroscopic investigations were carried out jointly. NEXAFS (near-edge absorption fine structure) spectroscopy is one of the effective techniques to study the electronic atomic and crystalline structure of materials. X-ray absorption process has a local character (associated with hole localization in the core shell) and dipole selection rules for the transitions between the initial and the final states have been worked out. Thus the possibility to obtain the information about local and partial density of electronic states of the conduction band is appeared.

2. Experimental details

TiO_2 films of 20-80nm thickness were grown by atomic layer deposition (ALD) technique on a top of the production-grade substrates (Ni or glass). ALD synthesis provides the thickness-control and the aggressive conformality of TiO_2 thin films at a reasonably low processing temperature.

The uniform transparent-conductive-oxide (TCO) buffer layer (ITO ($(In_2O_3)_{0.9}(SnO_2)_{0.1}$ or SnO_2 or ZnO) was used and grown on substrate prior to the ALD of TiO_2 film. The TiO_2 films were deposited in a cross-flow "Nanoserf" reactor at a temperature of 200º C using $TiCl_4$, $Ti(OCH(CH_3)_2)_4$, $[(CH_3)_2N]_4Ti$ and H_2O as a precursors.

The resistive switching behavior of the synthesized structures was measured at room temperature using an original setup in the I–V sweep mode (fig.1). The I-V curves of the sample were measured by applying a linearly varying current in the range of + / - 10 mA to the top electrode with the bottom electrode grounded. As for the ohmic contact to the TiO_2 and TCO layers the Cu, Au or Pt circular-shaped electrodes were used as external point contacts. The contact area was about $3x10^{-5}cm^2$. Voltage drop across the sample was changed within + / - 10 volts with increment of 12 mV, that allowed to create an electric field of the order of 1MV/cm in the TiO_2 layer. The experimental error connected with computer extrapolation of the data in the region of zero current at zero voltage was about 25 mV. The used setup also allowed registering a capacity (at 1 MHz AC) of the studied structures.

The quality of the synthesized structures was controlled by a scanning electron microscopy (SEM), a scanning ion microscope (SIM) and X-ray microanalysis. It was established for all the films the thickness uniformity better than 0.3 nm across the wafer.

The near edge X-ray absorption fine structure (NEXAFS) measurements were performed at the reflectometer set-up mounted on the optics beamline (D-08-1B2) at the Berlin Synchrotron Radiation facility BESSY-II of the HZB. A GaAsP diode, together with a Keithley electrometer (617), was used as a detector. NEXAFS spectra were measured at the incident angle of 45º in the vicinity of Ti $L_{2,3}$- and OK–absorption edges with energy resolution better than $E/\Delta E=3000$. The spectra were obtained by monitoring the total electron yield from the samples in a current mode.

It was developed and testified a special fiducial grid applied on the surface of the samples enabling to carry out the current-voltage measurements and spectroscopic studies in the same point of the film. Also the apertures were used to minimize the cross-section of X-ray beam and thus to narrow the area of light spot on the film to the size comparable to the Au electrode contact area. As consequence the obtained NEXAFS spectra provided information on changes in the electronic atomic structure itself from the electric field impact area.

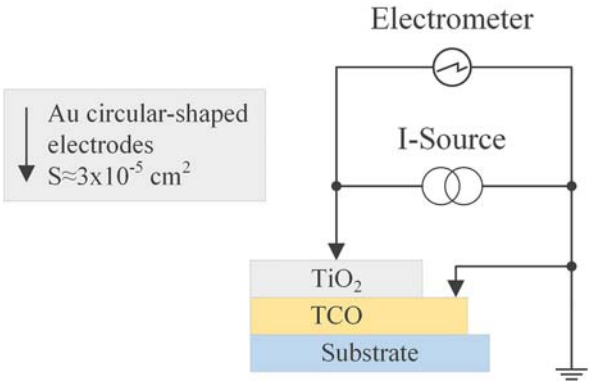

Figure 1. Circuit diagram of electrophysical measurements.

3. Results and discussion

It is known [8,10,18,27,28], that in the case of a single-oxide-layer structure (unlike bilayer structures consisting of non-stoichiometric oxide and oxide) the electroforming step of the pristine structure is required before a bistable switching is achieved. Often, the electroforming is a somewhat slower process than the actual switching. In point of fact the electroforming is the soft breakdown of the insulating oxide layer when the high electric field is applied to the structure. When high electric field is applied the oxygen atoms are knock out from the lattice and move to the electrode with the positive voltage creating defects that lead to formation of levels in band gap [29-33].

Impact of a strong electric field of the order 1MV/cm on the metal/TiO_2/TCO/metal structures was carried out by applying a negative bias to the top electrode (with the bottom electrode grounded) with an appropriate compliance current that leads to decrease in the initial resistance R_0 of the pristine structure (after synthesis) to R_H, which we will refer a high-resistance state (R_H).

3.1. Current (I)–voltage (V) studies of metal/TiO_2/TCO/metal assemblies

Fig. 2 (a) shows I-V curves for Au/TiO_2(20nm)/SnO_2/Au assembly. For this structure the initial resistance R_0 was reduced from R_0=50 kΩ to R_H=5-10 kΩ after electroforming step. The measurements reveal the asymmetric I-V loops with non-linear rectifying features following the voltage sweep 0 →V_{min}→0 →V_{max}→ 0 in sequence, shown by the arrows. Detailed analysis of the switching process in metal/TiO_2(20nm)/SnO_2/metal assembly shows that resistive switching from one state to another state in this structure occurs only by changing the polarity of the applied voltage (by applying a negative bias for R_H→R_L switching and only by applying the positive bias for R_L→R_H switching) and under conditions of a strong electric field applied to the TiO_2 layer (~ 1MV/cm). An increase in the absolute value of the bias potential reaches a certain threshold value above which the structure transfers from the R_L state into R_H state (or some intermediate states) and vice versa. The multiple resistive states realized in the structure and characterized by different values of the resistance for Au/TiO_2(20nm)/SnO_2/Au structure are shown in fig.2 (b). The observed deviation from the zero current at zero voltage (fig. 2b) may be related to the nanobattery effect as reported by [34]. However, the value of the observed deviation (about 25 mV) is comparable to the experimental error and computer extrapolation of the data in the region of zero voltage that does not allow confirm/refute the suggested supposition. Controlling the magnitude of the charge flowing through the structure during the process of the resistive switching one can discretely change the value of the resistance. It was established that transition from the high resistance state R_H to the low resistance state R_L occurs much faster, i.e. $\tau_{H\to L} \ll \tau_{L\to H}$ and was accompanied by an increasing a capacitance of the structure in half. The capacitance value remained virtually unchanged within the linear part of the I-V curve.

Thus formed structure turned out capable of storing R_H state for a long time or changes the value of resistance (increase of the slope of the I-V linear part curves) up to values of order R_L=250Ω, depending on the charge passing through the structure. This state we will refer a low resistance state with R_L. Change of the resistance value in the region of linear part of the I-V curve (change of the slope of the I-V linear part curves) was reversible, and the transition from the state with R_L to the state with R_H was accompanied by the occurrence of charge order of 3×10^{-2}C.

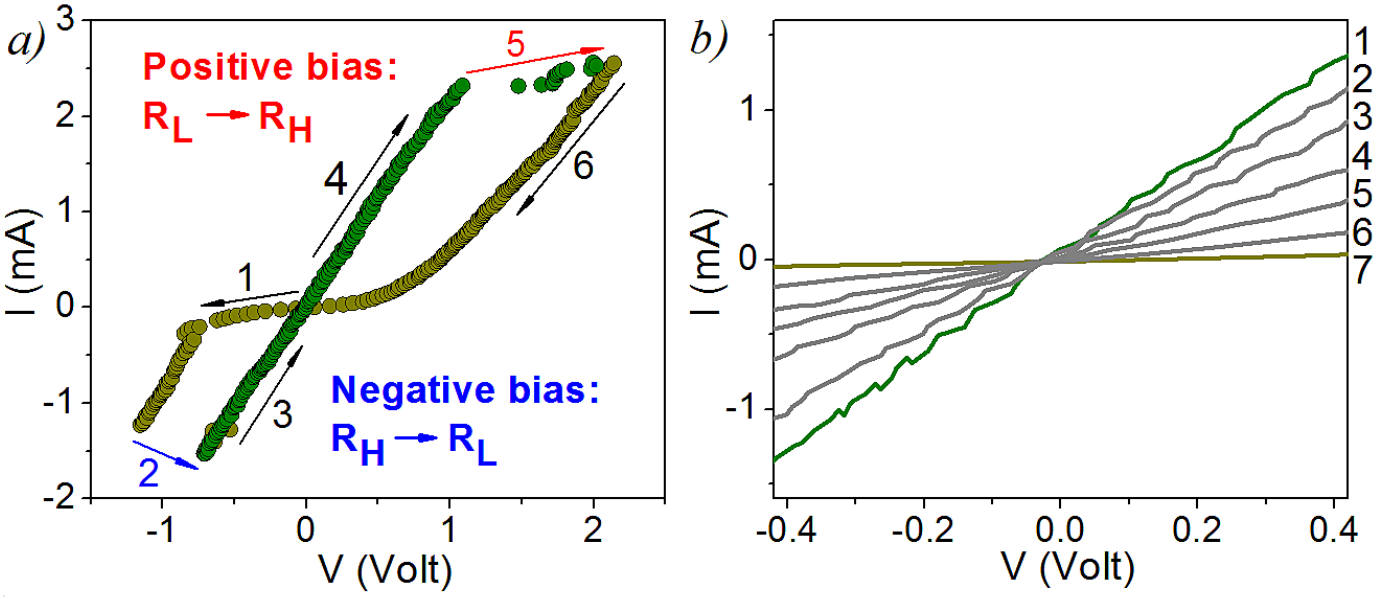

Figure 2. I-V characteristics of Au/TiO_2(20nm)/SnO_2/Au assembly (arrows indicate the direction of the circuit, the colored arrows correspond to transition between resistive states) showing clockwise bipolar resistive switching (a) ; multiple resistive states of the structure characterized by different values of the resistance (b) : 1 corresponds to minimum value of the resistance R_L=300 Ω; 7 corresponds to maximum value of the resistance R_H=10 kΩ; 2-6 – correspond to intermediate resistance values.

The dependences of the resistance R_L and R_H on the electrode material are illustrated in the fig.3 on an example of metal/TiO_2(20nm)/SnO_2/metal assembly. It was established that the R_L is independent on the electrode material that allows to conclude that in the R_L state the conductivity of the structure is completely determined by the charge carriers transport on the conducting paths in the TiO_2. As opposed to R_L, the resistance value R_H depends on the used electrode material: the maximum resistance value R_H was observed in the case of Pt electrodes.

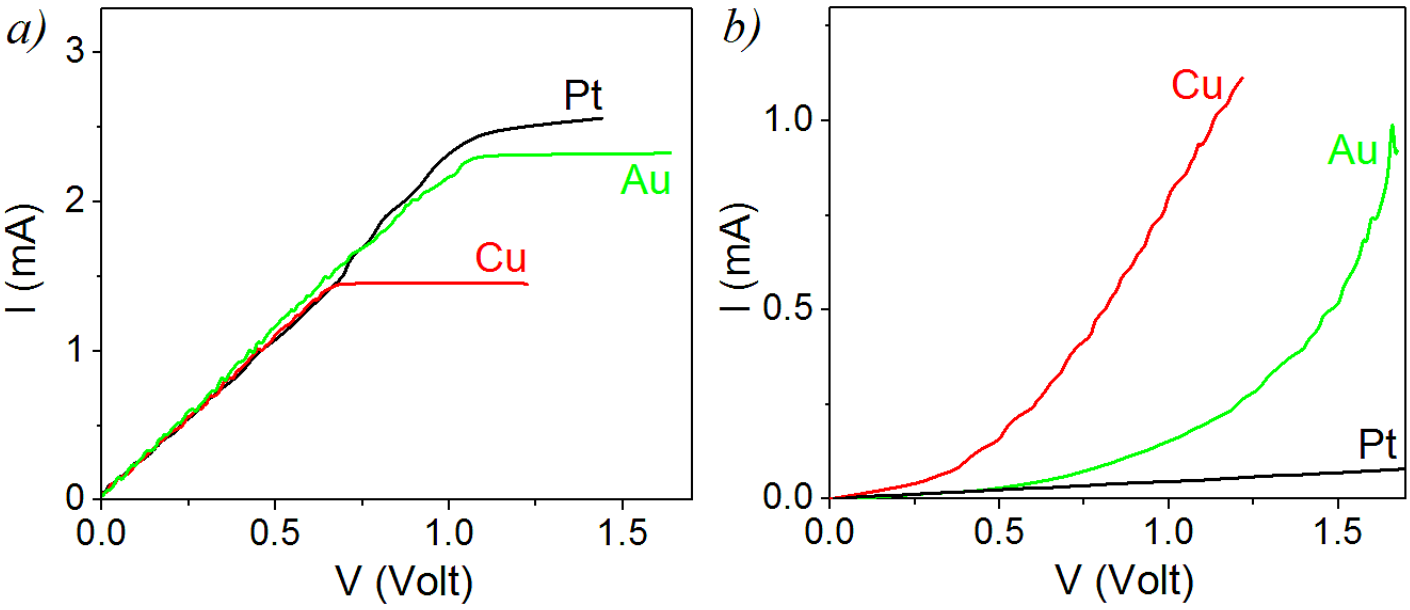

Figure 3. Dependence of the resistance R_L (a) and R_H (b) on the electrode material for metal/TiO_2(20nm)/SnO_2/metal assembly.

Since the influence of moisture on the resistive switching process has been pointed out by [35] and especially the influence of different electrode materials on the OFF state resistance and ionic concentration in presence of moisture [36] we have also carried out additional studies using a special hermetic box filled with nitrogen. It was established that atmosphere composition where the measurements are carried out and presence/absence of moisture do not effect on the discussed resistive switching and on its characteristics (switching voltage, the resistance values of R_L and R_H states, etc.). Based on this observation and fact that TCO is additional source of oxygen vacancies we can suppose that conductivity in R_L state is due to formation of conducting filaments composed by oxygen vacancies rather than mobile metallic cations as in case of Cu/SiO_2/Pt [35] for which influence of moisture is critical.

Also the resistive switching behavior in the Au/TiO_2(20nm)/SnO_2/Au assembly on the way of influence on the structure was studied. It was established that the number of switches between different states depends strongly on the method used. As follows from fig. 4 (a), while continuously measured I-V (continuous applying a linearly varying bias voltage) characteristics only the 10-20 complete switching cycles ($R_L \rightarrow R_H \rightarrow R_L$) were observed. When applying the current pulse a much larger number of complete cycles of switching (fig.4 (b)) were achieved, and, that most importantly, the degradation of the sample was not observed in this case. The obtained resistive states persist at least during 60 hours.

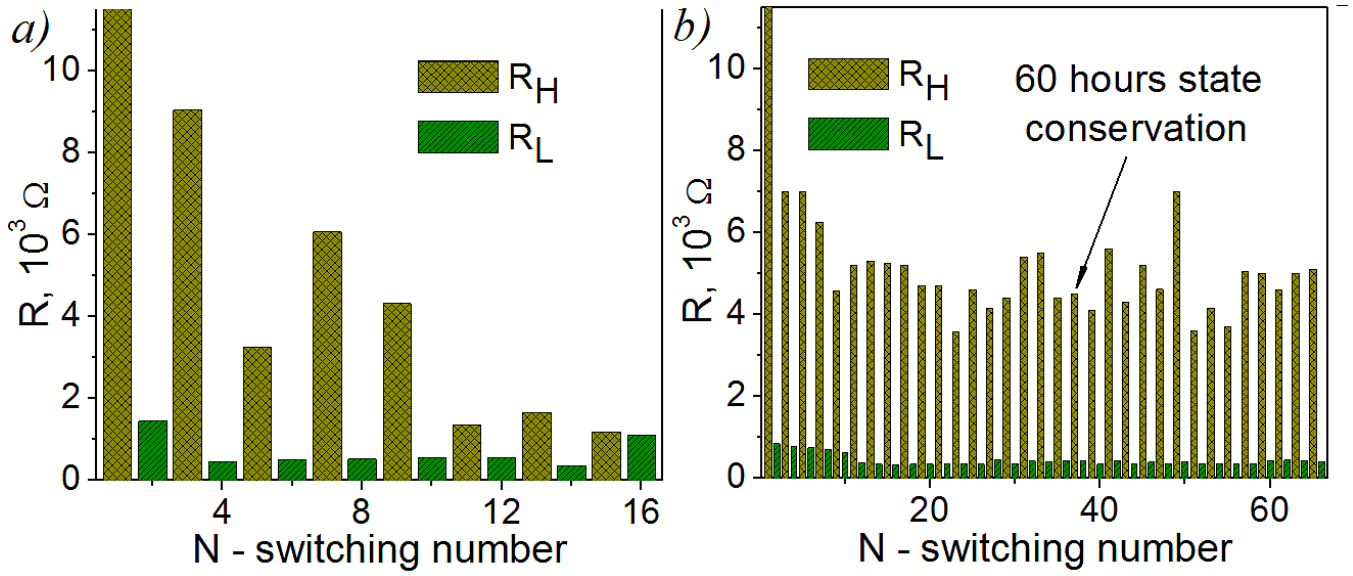

Figure 4. Dependence of the R_L and R_H states on the number (N) of resistive switching in the Au/TiO_2/SnO_2/Au assembly obtained by: (a) continuous applying a linearly varying bias voltage, (b) applying the current pulse.

Analogous conclusions have been made in the study of Au/TiO_2(30nm)/ZnO/Au assembly. I-V characteristics for Au/TiO_2(30nm)/ZnO/Au assembly are shown in fig.5.

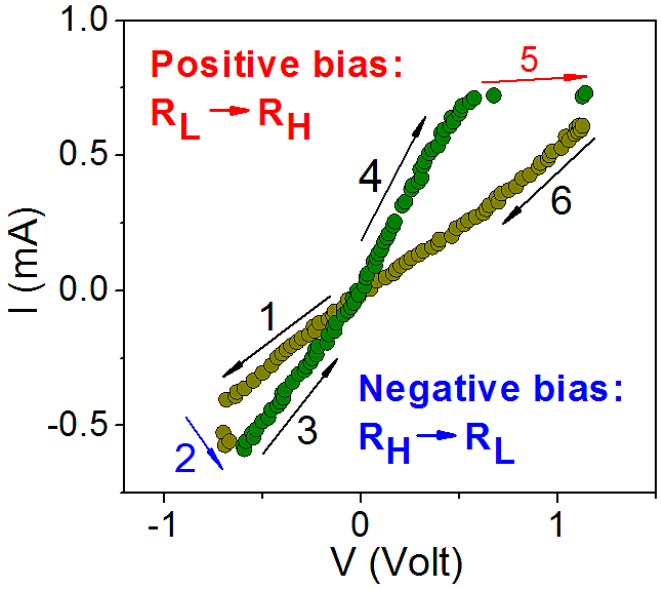

Figure 5. I-V characteristics of Au/TiO_2(30nm)/ZnO/Au assembly (arrows indicate the direction of the circuit, colored arrows correspond to transition between resistive states) showing clockwise bipolar resistive switching.

I-V curves of Au/TiO_2(25nm)/ITO/Au assemblies without/with Al_2O_3 layer inserting between TiO_2 and ITO layers are shown in fig. 6 and 7. The joint analysis of I-V characteristics of all the studied assemblies reveals the possibility of implementing anti-clockwise bipolar resistive switching only in the Au/TiO_2/ITO/Au assembly. It is important that insertion of thin Al_2O_3 layer between TiO_2 and ITO layers does not permit to realize the anti-clockwise bipolar resistive switching.

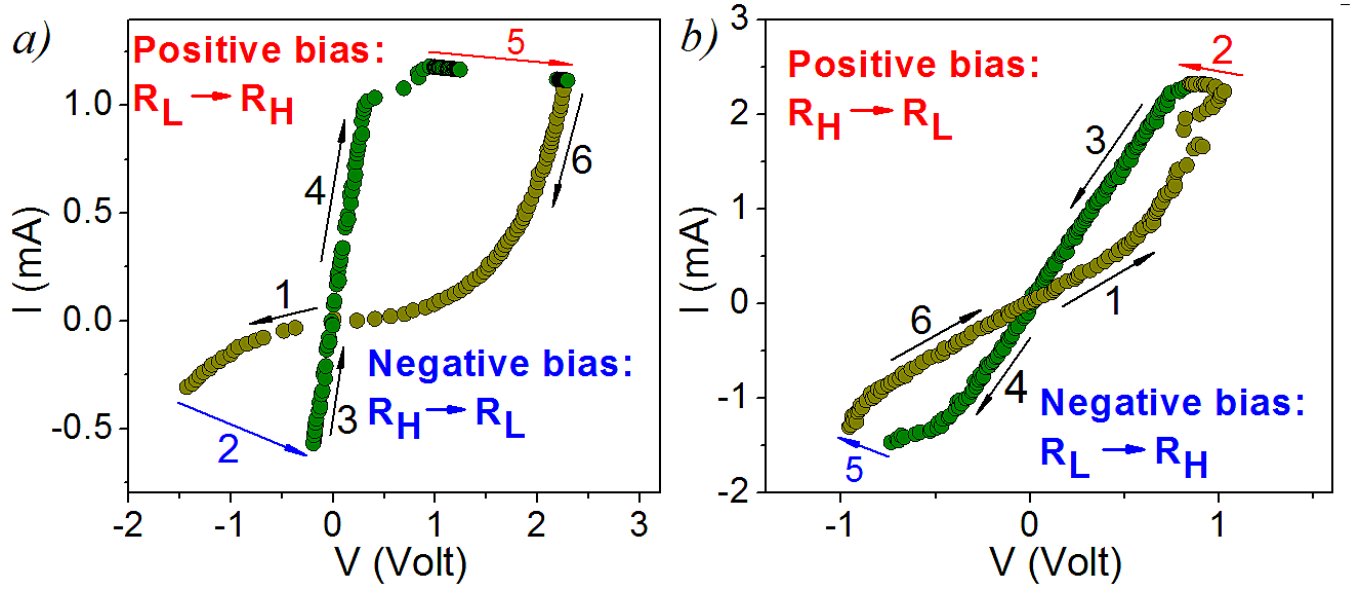

Figure 6. I-V characteristics of Au/TiO_2(25nm)/ITO/Au assembly (arrows indicate the direction of the circuit, colored arrows correspond to transition between resistive states) showing clockwise bipolar resistive switching (a) and anti-clockwise bipolar resistive switching (b).

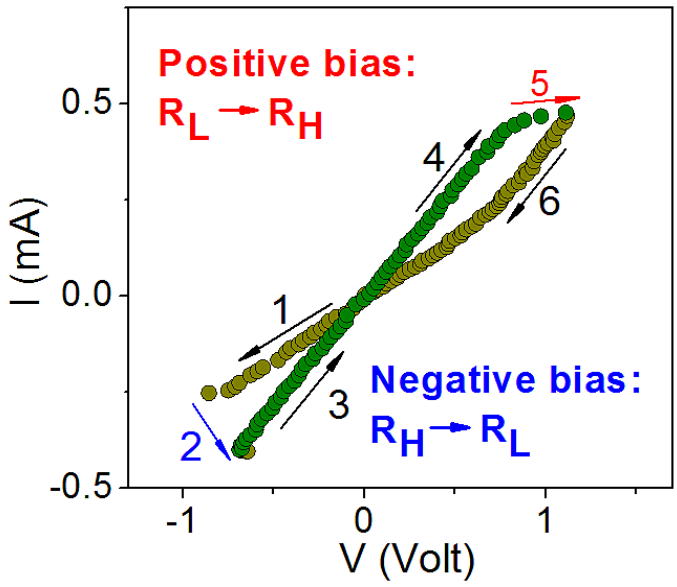

Figure 7. I-V characteristics of Au/TiO_2(25nm)/Al_2O_3(5nm)/ITO/Au assembly (arrows indicate the direction of the circuit, colored arrows correspond to transition between resistive states) showing clockwise bipolar resistive switching.

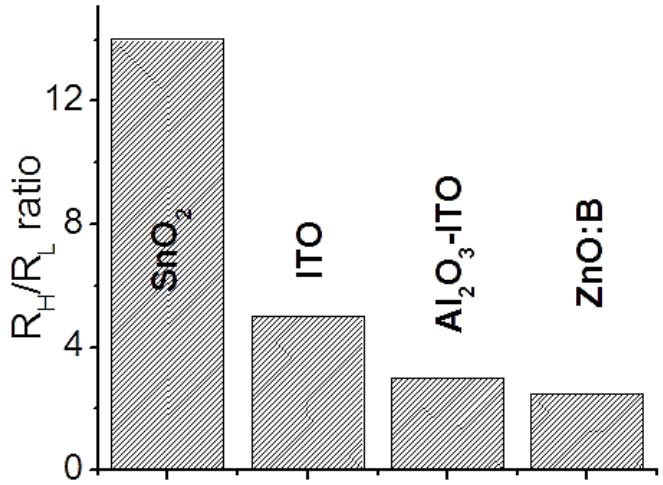

Figure 8. Average R_H/R_L ratio for studied assemblies.

Summing up the results of current–voltage analysis let us turn to the fig.8 where the average R_H/R_L ratio for all the studied assemblies is shown. One can see that the greatest value of the ratio R_H/R_L is observed for assembly with SnO_2 buffer layer. From the viewpoint of practical use of memristor memory this means that it possible to implement the maximum set of intermediate states (recording analog data) and increases the density of information recording in this case. That is what allows to give preference to sublayer SnO_2.

Based on the obtained set of current (I)–voltage (V) results, we tried to make preliminary conclusions about the possible mechanisms of resistive switching process. As was mentioned above the electroforming step of the pristine structure, which is required before bistable switching is achieved. The electroforming process is accompanied by formation of the levels in the band gap (appearance of an additional conduction channel due to the formation of electronic states in the band gap of insulator). As a result the conductivity of the structure in the state R_H is defined by two processes: conductivity by these levels and conductivity by conduction band on Schottky-like transport mechanism. This is evidenced by reducing the impact of emissions through the Schottky-like barrier at the interface TiO_2 - metal with increasing the work function of the electrode used (fig.3, (b)).

The independence of the resistance R_L on the electrode material i.e. work function (fig.3, (a)) allows us to suggest that in the R_L state the conductivity of a structure is completely determined by the charge carriers transport in the levels in the band gap of TiO_2. Such assumption agrees well with [37]. According to [37], the formation of complexes containing oxygen vacancies: $(Ti^{3+} - V_o + 2e)^0$ and $(Ti^{3+} - V_o^+ + 1e)^+$ is typical for TiO_2 layers. Such complexes lead to the formation of the energy levels in the band gap located at ~0.3 eV and ~0.5 eV below the bottom of the conduction band [37]. It is plausible to associate R_L state of the structure with the presence of the maximum concentration of the oxygen vacancies in the TiO_2 layer, which may form conductive path of oxygen vacancies, so called conductive filaments. A significant increase in the resistance of the structure (from ~10 Ω to ~100 kΩ) after annealing in oxygen atmosphere is an additional proof of our assumption. Taking into account: i) a significant difference in the switching process in the chain $R_H \rightarrow R_L \rightarrow R_H$; ii) a remarkably different inertia of the processes $\tau_{H \rightarrow L} << \tau_{L \rightarrow H}$; iii) a different behavior of the intermediate states, it is reasonable to assume that the increasing (transition $R_H \rightarrow R_L$) and reduction (transition $R_L \rightarrow R_H$) of conductance occur due to different mechanisms.

3.2. NEXAFS study of Au/TiO_2/ITO/Au and Au/TiO_2/Al_2O_3/ITO/Au assemblies

The absorption spectra in the vicinity of titanium $L_{2,3}$- and oxygen K-absorption edges were measured for all the samples with ITO ($(In_2O_3)_{0.9}(SnO_2)_{0.1}$) TCO buffer layer. It should be noted that the Ti $L_{2,3}$- absorption spectra for all the studied samples (before and after switching) were almost indistinguishable and corresponded to the spectrum of the amorphous TiO_2 film. That means that the main changes of the structure occur in the sublattice of oxygen. Therefore further the OK-absorption spectra will be discussed only.

Fig. 9 shows the OK-absorption spectra of the studied films (pristine structure). The relative intensities of all the spectra have been normalized to the continuum jump (at the photon energy of 560 eV for O1s absorption spectra) after subtraction of a sloping background, which was extrapolated from the linear region below O1s absorption onset. Such normalization provides about the same total oscillator strength for all the O1s-absorption spectra over the photon energy range of 520-560 eV in accordance with a general idea of oscillator strength distribution for the atomic X-ray absorption [38]. It is important to emphasize that all the samples were studied at different points of the structure. It was established for each sample that within the statistical error (on the order of 3%) the spectra measured at different points on the surface of the sample coincided.

According to [39-40] the molecular orbitals of TiO_2 derived from a linear combination of atomic orbitals (LCAO) are characterized by four unoccupied orbitals: $2t_{2g}$(Ti 3d + O 2pπ), $3e_g$(Ti 3d + O 2pσ), $3a_{1g}$(Ti 4s + O 2p) and $4t_{1u}$(Ti 4p + O 2p). In TiO_2, all four molecular orbitals are completely empty. In this classification the O K-edge features (labeled as ***a***, ***b***, ***c*** and ***d***) can be assigned to one electron transitions from the O 1s orbital to the $2t_{2g}$, $3e_g$, $3a_{1g}$ and $4t_{1u}$ orbitals of TiO_2, respectively. Thus ***a*** and ***b*** peaks reflect the core-electron transitions in the oxygen atoms to the lowest unoccupied Ti 3d-t_{2g} and 3d-e_g electronic states that are mixed with the 2p states of the ligand (oxygen) atoms. As it follows from fig. 9, the spectra for all the studied films correlate well in number and energy position of the main details of the structure. Analysis of the energy position of the peaks shows that within the experimental accuracy (10 meV) the energy separation between ***a*** and ***b*** peaks ΔE_{a-b}=2.2 eV is closed to the value for the amorphous TiO_2 (2.3eV) [41-42]. At the same time the appreciable decrease of the main band integral intensity (including ***a*** and ***b*** peaks) depending on the material of the buffer layer is traced and is likely a result of the varying of oxygen content in synthesized TiO_2 films. As it follows from fig. 9, the lowest intensity of this band occurs in the film grown onto ITO layer that is likely a result of formation of film with lowest stoichiometry during synthesis due to migration of oxygen ions from TiO_2 film into ITO since the structure of ITO contains considerable number of oxygen vacancies [43]. An additional evidence of this conjecture can be found in the second band characterized by ***c*** and ***d*** peaks and related to transitions into the empty electronic states with mixed Ti 4s,4p + O 2p character. Analysis of the O K-absorption spectra [41-42, 44-47] points to the significant differences of the features at the higher energies for different crystal modifications and amorphous phase of TiO_2. The less pronounced splitting the ***c*** and ***d*** peaks confirms the lowest stoichiometry of the film grown onto ITO buffer layer. The use of the Al_2O_3 blocking layer allows to restrict to some extent processes of migration of oxygen ions and vacancies as it follows from work [48-49]. This fact agrees well with our results since the main band integral intensity has a higher value and more pronounced splitting of the ***c*** and ***d*** features is traced in the spectrum of the TiO_2/Al_2O_3/ITO assembly (fig. 9) as compared with TiO_2/ITO assembly.

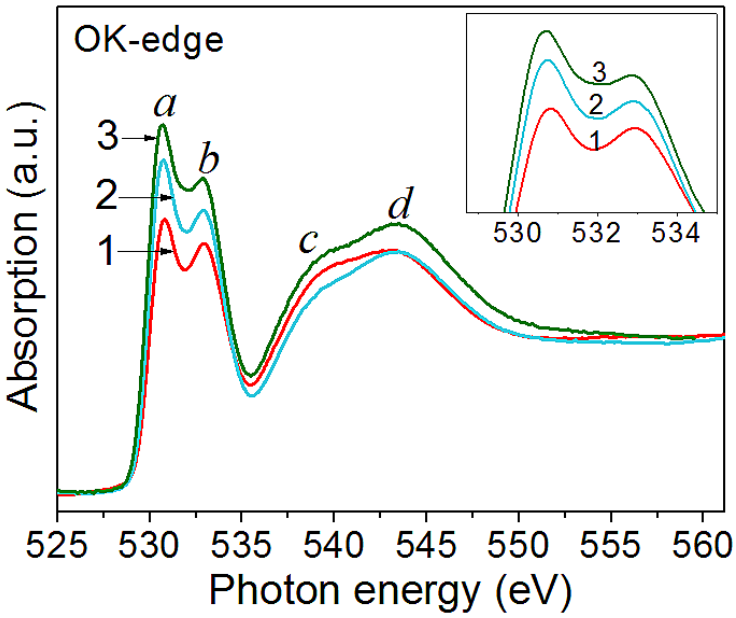

Figure 9. OK-absorption spectra of the TiO_2/ITO (1), TiO_2/Al_2O_3/ITO (2) and TiO_2/SnO_2 (3) assemblies (pristine structure).

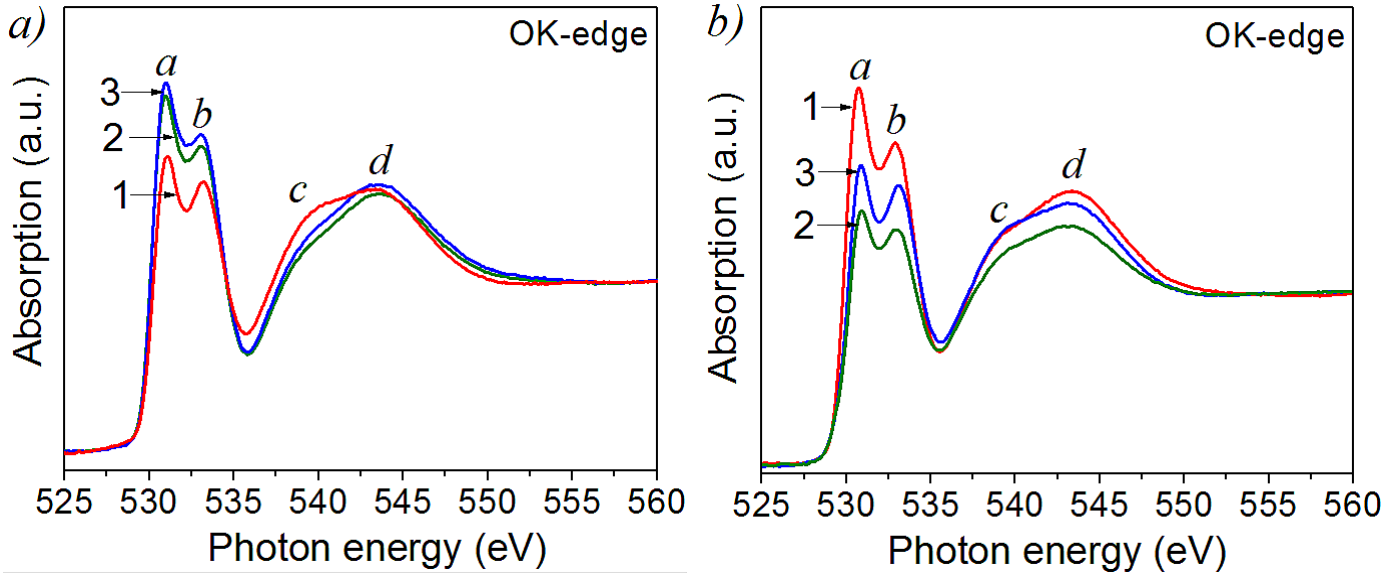

Figure 10. OK-absorption spectra of the TiO_2/ITO (*a*) and TiO_2/Al_2O_3/ITO (*b*) assemblies after $R_H \rightarrow R_L$ transition (2) (negative polarity of applied voltage) and $R_L \rightarrow R_H$ transition (3) (positive polarity of applied voltage) to compare with OK-absorption spectra of the pristine structures (1).

Fig. 10 demonstrates the OK-absorption spectra of the TiO_2/ITO and TiO_2/Al_2O_3/ITO assemblies before (pristine structure) and after resistive switching. As it can be seen from fig. 10 the main band integral intensity is appreciably changed after switching that can be related with changes in sublattice of oxygen. In case of the TiO_2/ITO assembly (fig. 10 (a)) the main band integral intensity is increased and features ***c*** and ***d*** become more distinguishable for both R_H and R_L states. This can be related presumably with some restoration of stoichiometry of the TiO_2 film after the resistive switching due to reverse migration of oxygen ions from ITO that may be launched under the influence of local heating in the area of high electric field. Effect of the migration of oxygen ions from ITO can be overlapped with effects related directly with process of resistive switching (the spectra for R_H and R_L states are almost indistinguishable with slight predominance of main band integral intensity for R_H state). In this connection the

analysis of OK-absorption spectra of TiO_2/Al_2O_3/ITO assembly can give more direct information about process of resistive switching since buffer layer of Al_2O_3 considerably restricts migration of oxygen as it mentioned above.

It can be seen from fig. 10 (b) that the forming process and irreversible conversion of TiO_2 film from R_0 to R_H state in the TiO_2/Al_2O_3/ITO assembly is accompanied by decrease of the main band integral intensity of the OK-absorption spectrum and the splitting of features ***c*** and ***d*** becomes less pronounced. This can be related with general reduction of stoichiometry of TiO_2 film and formation of scattered oxygen vacancies that lead to formation of energy levels in band gap. The transition of the film into conductive state is accompanied by a further decrease in the main band integral intensity of the OK-absorption spectrum. In our opinion the transition $R_H \rightarrow R_L$ is caused by the formation of conductive path formed by oxygen vacancies in TiO_2 film in the area of localization of high electric field as a result of thermal ejection of oxygen ions from regular bonding. Electric field violates the symmetry of the potential barrier and reduces its height in the direction of the field on Schottky-like mechanism that additionally facilitates ejection of oxygen ions from the regular bonding. The negative polarity of the applied voltage at $R_H \rightarrow R_L$ transition provides displacement of the oxygen ions from the region of the localization of produced vacancy, excluding the possibility of reuptake. In essence, the joined effect of local heating and electric field disturbs the balance between release of the oxygen ions and their reuptake. In this case, an increase in conductivity of the structure is associated presumably with the formation of filaments of the oxygen vacancies. Since the reuptake of oxygen ions is significantly impeded, it is unlikely to expect even short-term reduction in the conductivity that correlates well with rapid character of $R_H \rightarrow R_L$ transition observed in the experiment (fig. 6 (a)).

For conducting a $R_L \rightarrow R_H$ transition it is necessary to break conducting pass formed by oxygen vacancies and reduce a general number of vacancies that correlates with increased main band integral intensity for R_H state to compare with R_L state (fig. 10 b). This requires to implement more complex and combined processes consisting in the shipping and/or the formation of an oxygen ions in the region of the conductive path localization (or complexes described above) with subsequent its capture and forming a regular (may be distorted) bonding Ti-O. At least two-stage of the process significantly increases its inertia. The slowest step in this case is the formation of oxygen ions in the region of the oxygen vacancies localization. Moreover, this process not just can, but must be accompanied by a process of vacancy formation described above, as occurs in the conditions of the joint action of the electric field and the local heating. This was observed in the short-term fluctuations of the conductivity of the system for certain values of the electric field, established in the experiment (fig. 6 (a)).

Local heating process at this stage plays a dual role. On the one hand, it can promote the increase in the concentration of oxygen ions due to the diffusion and it is a positive factor. On the other hand, the self-heating process initiates the formation of oxygen vacancies, which in this case is a negative factor.

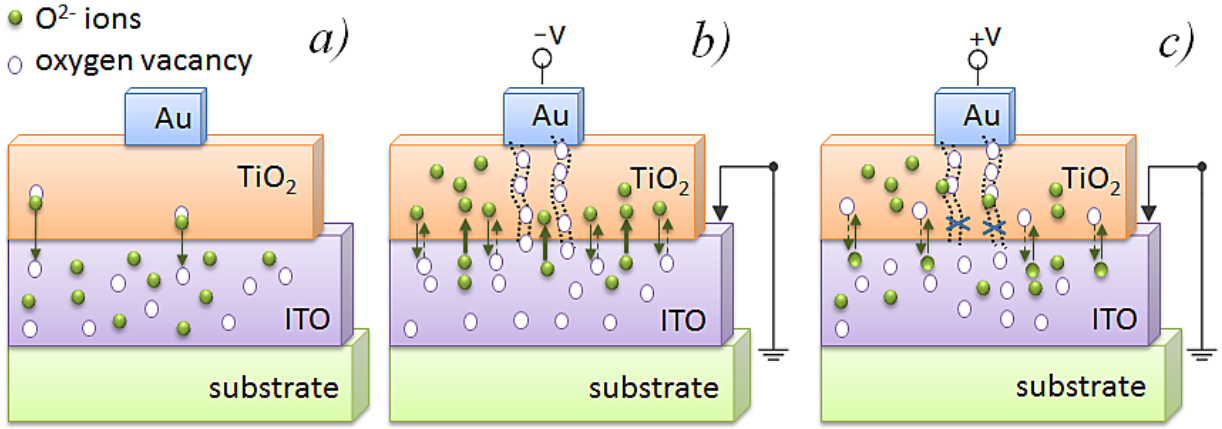

Figure 11. Schematic diagram of the conduction mechanism in the TiO_2/ITO assembly: a) pristine structure; b) formation of conducting path $R_H \rightarrow R_L$; c) rupture of conducting path $R_L \rightarrow R_H$. Solid arrows show the movement of oxygen ions (green circles). Dotted arrows show the movement of oxygen vacancies (white circles). The thickness of the arrows indicates the intensity is proportional the flow quantity.

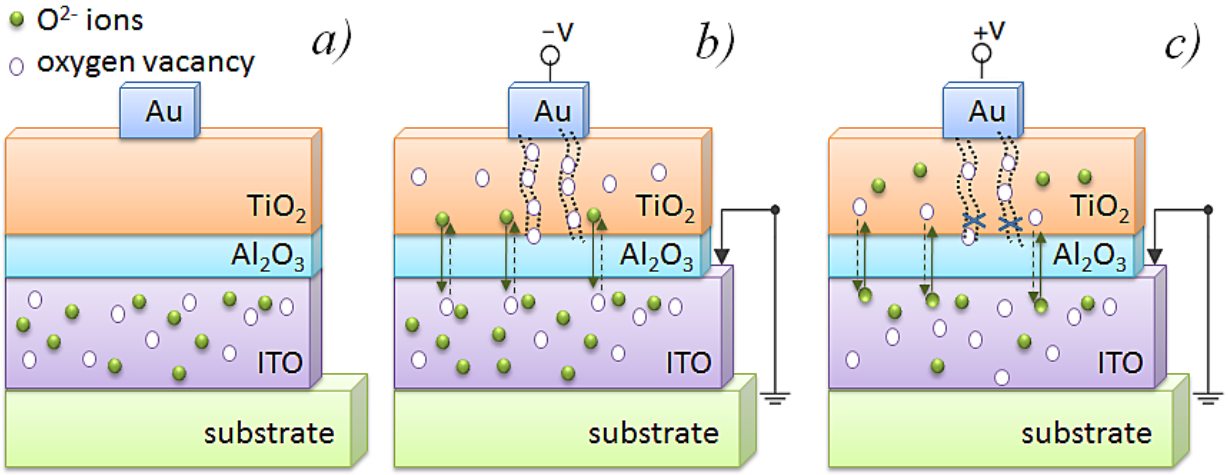

Figure 12. Schematic diagram of the conduction mechanism in the TiO_2/Al_2O_3/ITO assembly: a) pristine structure; b) formation of conducting path $R_H \rightarrow R_L$; c) rupture of conducting path $R_L \rightarrow R_H$. Solid arrows show the movement of oxygen ions (green circles). Dotted arrows show the movement of oxygen vacancies (white circles).

Schematic diagrams shown in the figs. 11 (a-c) and 12 (a-c) summarize the mechanism of conductivity modulation during resistive switching in the TiO_2/ITO and TiO_2/Al_2O_3/ITO assemblies. Figs. 11 (a) and 12 (a) illustrate the state of the pristine structure. As was mentioned above that the TiO_2 film grown onto ITO buffer layer is characterized by lowest stoichiometry compared with the film prepared onto Al_2O_3/ITO buffer layer. Taking into account that the ITO layer contains a surplus of the oxygen vacancies [43] (white circles) it is reasonable to assume that the O^{2-} ions (green circles) will be easily move from TiO_2 into ITO layer within the interface region under the influence of the internal electric field (this process is indicated by solid arrows). Al_2O_3 acts as a barrier layer against arbitrary migrations of charged particles [48-49].

Fig. 11 (b) illustrates the state of the TiO_2/ITO assembly when a negative bias is applied to the top electrode and the bottom electrode is grounded. In this case the O^{2-} ions penetrate through the barrier at the TiO_2/ITO interface into ITO layer leaving behind vacancies. The oxygen vacancies in ITO side serve as the trap sites for the O^{2-} ions (dotted arrows). Simultaneously, there is a process of reverse migration of O^{2-} ions from ITO under the influence of the local heating (thick solid arrows). As the result, the low resistance state R_L (characterized by high conductivity) is achieved with formation of electrically conductive path formed presumably by oxygen vacancies (dotted lines) which are surrounded by oxygen ions from ITO. The electric field (negative polarity applied to the top electrode onto TiO_2 film) prevents the merger of oxygen ions and vacancies. When positive bias is applied to the top electrode and reaches certain threshold value the state of the high resistance R_H is realized (fig 11 (c)). O^{2-} ions get trapped in the ITO layer moving back towards the TiO_2 film, which leads to a rupture of the conduction channel in the vicinity of the interface and oxygen vacancies are against get distributed in the ITO layer. It is worth noting that removal of a small amount of the O^{2-} ions is sufficient to break the conduction path and thereby to increase the resistance.

Similar processes occur during the resistive switchings in the TiO_2/Al_2O_3/ITO assembly (fig. 12 (b-c)). But in this case, the Al_2O_3 prevents a spontaneous movement of the oxygen ions and vacancies in the absence of the electric

field and regulates their movement when the high electric field is applied. The introduction of the Al_2O_3 buffer layer allows to increase the temporal stability of the R_L and R_H states of the film [48]. In the R_L state the reverse migration of the O^{2-} ions from the ITO layer into the film is shuted by the alumina barrier. O^{2-} ions drift towards ITO leaving behind vacancies under negative electric field (fig. 12 (b)). The reverse migration of O^{2-} ions from ITO into the film shut by alumina barrier. So, concentration of oxygen into TiO_2 film decreases as evidenced by a decrease in intensity of the details ***a-b*** in the OK-edge of absorption spectrum (fig. 10 (b)). Under the application of electric field of positive polarity removing of O^{2-} ions towards TiO_2 film break the conduction path (fig. 12 (c)) and the oxygen concentration slightly increases (fig. 10 (b) 3-rd curve).

4. Conclusion

As it was mentioned in the introduction, the use of a thin buffer layer between dielectric film and substrate allows to affect the self-organization of the film. Taking into account a high concentration of oxygen vacancies in transparent-conductive-oxide (TCO) layers we have assumed that TCO layer in metal/TiO_2/TCO/metal assembly could be an additional source of oxygen vacancies for TiO_2 film. In this connection the metal/TiO_2/TCO/metal assemblies were synthesized. The resistive switching process has been studied in the metal/TiO_2/TCO/metal assemblies depending on the material of TCO (ITO ($(In_2O_3)_{0.9}(SnO_2)_{0.1}$ or SnO_2 or ZnO). The current work first time combines both the electro-physical studies and x-ray near-edge absorption fine structure (NEXAFS) investigations. It was established that switching process influences strongly the lowest unoccupied bands and local atomic structure of the TiO_2 layers. It was established that TCO layer in metal/TiO_2/TCO/metal assemblies is an additional source of oxygen vacancies for TiO_2 film. The R_L (R_H) states are achieved with formation (rupture) of electrically conductive path of oxygen vacancies correspondingly. The resistive switching leads to some restoration of stoichiometry of the film in the TiO_2/ITO assembly. A clockwise and anti-clockwise bipolar resistive switching is realized only in the Au/TiO_2/ITO/Au assembly. The inserting the Al_2O_3 thin layer allows to restrict to some extent processes of migration of oxygen ions and vacancies and does not permit to realize the anti-clockwise bipolar resistive switching. A greatest value of the ratio R_H/R_L is observed for assembly with SnO_2 buffer layer. It was established that a remarkably different inertia is a characteristic for increasing (transition $R_H \rightarrow R_L$) and reduction (transition $R_L \rightarrow R_H$) of conductance $\tau_{H \rightarrow L} << \tau_{L \rightarrow H}$. Applying the current pulse provides a much larger number of complete cycles of switching unlike continuous applying of linearly varying bias voltage; the obtained resistive state persists at least during 60 hours. The obtained results are very important for deeper understanding the mechanism of resistance switching and charge transport in TiO_2 films and its future application as switching material in resistance change memory based devices.

Acknowledgments

The work was supported by St. Petersburg State University Grant 11.37.656.2013. The authors gratefully acknowledge the assistance from the Helmholtz Zentrum Berlin (HZB). Also the authors gratefully acknowledge Prof. A.S. Shulakov for fruitful discussions. The work performed using equipment of interdisciplinary resource center for "Nanotechnology" and resource center "Innovative technologies of composite nanomaterials" of St. Petersburg State University.

References

[1] Szot K et al 2006 *Nature Mater* **5** 312–320

[2] Aono M et al 2005 *Nature* **433** 47–50

[3] Mead C 1989 *Analog VLSI and Neural Systems* (Addison-Wesley, Reading, MA)

[4] Boahen K 2005 *Neuromorphic microchips. Sci. Am.* **292** 56–63

[5] Strukov D B, Snider G S, Stewart D R and Williams R S. 2008 *Nature* **453** 80

[6] Strukov D B and Williams R S 2009 *Appl. Phys. A* **94** 515

[7] Yang J J, Pickett M D, Xuema Li, Douglass AA Ohlberg, Stewart D R and R Stanley Williams 2008 *Nature nanotechnology* **3** 429

[8] Waser R, Dittmann R, Staikov G and Szot K 2009 *Adv. Mater* **21** 2632-2663

[9] Burr G W, Kurdi B N, Scott J C, Lam C H, Gopalakrishnan K and Shenoy R S 2008 *IBM J. RES. & DEV.* **52** no. 4 449-464

[10] Wong P H-S, Lee H-Y, Yu S, Chen Y-S, Wu Y, Chen P-S, Lee B, Chen F T and Tsai M-J 2012 *Proceedings of the IEEE* Vol. **100** no. 6 1951-1970

[11] Kim K M, Choi B J and Hwang C S 2007 *Appl. Phys. Lett.* Vol. **90** 242906

[12] Goux L, Lisoni J D, Jurczak M, Wouters D J and Courtade L 2010 *J. Appl. Phys.* Vol. **107** 024512

[13] Ielmini D, Nardi F and Cagli C 2011 *Nanotechnology* Vol. **22** 254022

[14] Goux L, Chen Y-Y, Pantisano L, Wang X-P and Groeseneken G 2010 *Electrochemical and Solid-State Letters* Vol. **13** no. 6 G54-G56

[15] Mehonic A, Cueff S, Wojdak M, Hudziak S and Jambois O 2012 *Journal of Applied Physics* Vol. **111** 074507

[16] Sun X, Li G, Zhang X, Ding L and Zhang W 2011 *J. Phys. D: Appl. Phys.* vol. **44** no. 12 1-5

[17] Janousch M, Meijer G I, Staub U, Delley B and Karg S F 2007 *Adv. Mater* vol. **19** 2232-35

[18] Yang J J, Strukov D B and Stewart D R 2013 *Nature Nanotechnology* vol. **8** 13-24

[19] Seok J Y et al 2012 *IEEE Electron Device Letters* **33** 582

[20] Kwon D-H et al 2010 *Nature nanotechnology* **5** 148-153

[21] Waser R 1991 *J. Am. Ceram. Soc.* **74** 1934

[22] Kim K M, Jeong D S and Hwang Ch S 2011 *Nanotechnology* **22** 254002

[23] Yoshida C, Tsunoda K, Noshiro H and Sugiyama Y 2007 *Appl. Phys. Lett*. vol. **91** 223510

[24] Filatova E O, Sokolov A A, Egorova Yu V, Konashuk A S, Vilkov O Yu, Gorgoi M and Pavlychev A A 2013 *J. Appl. Phys.* **113** 224301-8

[25] Filatova E O, Kozhevnikov I V, Sokolov A A, Egorova Yu V, Konashuk A S, Vilkov O Yu, Schaefers F, Gorgoi M and Shulakov A S 2013 *Microelectronic Engineering* **109** 13–16

[26] Filatova E O, Kozhevnikov I V, Sokolov A A, Konashuk A S, Schaefers F, Popovici M and Afanas'ev V V *J. Electron Spectroscopy & Rel. Phenom*. in print

[27] Jeong D S, Schroeder H, Breuer U and Waser R. 2008 *J. Appl. Phys*. vol. **104** 123716

[28] Yang J J, Miao F, Pickett M D, Ohlberg D A and Stewart D R 2009 *Nanotechnology* vol. **20** 215201

[29] Kim K M, Choi B J, Shin Y C, Choi S and Hwang C S 2007 *Appl. Phys. Lett.* **91** 012907

[30] Sato Y, Kinoshita K, Aoki M and Sugiyama Y 2007 *Appl. Phys. Lett.* **90** 033503

[31] Choi B J et al 2005 *J. Appl. Phys.* **98** 033715

[32] Rohde C et al 2005 *Appl. Phys. Lett.* **86** 262907

[33] Russo U, Ielmini D, Cagli C and Lacaita A L 2009 *IEEE Trans. Electron. Dev.* **56** 193–200

[34] Valov I, Linn E, Tappertzhofen S, Schmelzer S, Hurk J, Lentz F and Waser R 2013 *Nat. Commun.* **4** 1771

[35] Tappertzhofen S, Valov I, Tsuruoka T, Hasegawa T, Waser R and Aono M 2013 *ACS Nano* **7** 6396-6402

[36] Tappertzhofen S, Waser R and Valov I 2014 *ChemElectroChem* **1** 1287-1292

[37] Goepel W, Rocker G 1983 *Phys. Rev. B* **28** 3427

[38] Fano U and Cooper J W 1968 *Rev. Mod. Phys.* **40** 441

[39] Fischer D W 1972 *Phys. Rev. B* **5**(11) 4219

[40] Stoyanov E, Langenhorst F and Steinle-Neumann G 2007 *Am. Mineral.* **92** 557

[41] Rath S, Gracia F, Yubero F, Holgado J P, Martin A I, Batchelor D and Gonzalez-Elipe A R 2003 *Nucl. Instrum. Methods Phys. Res. B* **200** 248–254

[42] Filatova E, Taracheva E, Shevchenko G, Sokolov A, Kozhevnikov I, Yulin S, Schaefers F and Braun W 2009 *Phys. Status Solidi B* **1** 5

[43] Gabriela B G. 2012 *Materials* **5** 818-850

[44] Ruus R, Kikas A, Saar A, Ausmees A, Nommiste E, Aarik J, Aidla A, Uustare T and Martinson I 1997 *Solid State Commun.* **104**(4) 199–203

[45] F M F de Groot, Faber J, Michiels J J M, Czyzyk M T, Abbate M and Fuggle J C 1993 *Phys. Rev. B* **48** 2074

[46] Brydson R, Sauer H, Engel W, Thomas J M, Zeitler E, Kosugilland N and Kurodall H 1989 *J. Phys.: Condens. Matter* **1** 797–812

[47] F M F de Groot, Fuggle J C, Thole B T and Sawatzky G A *Phys. Rev. B* **41** 928

[48] Memory cell, Patent Russian Federation 2256957

[49] Konyushenko M A, Konashuk A S, Sokolov A A, Schaefers F and Filatova E O *J. Elec. Spectrosc. Relat. Phenom.*, in print